Available online at BCREC website: https://bcrec.id

Bulletin of Chemical Reaction Engineering & Catalysis, 17 (4) 2022, 755-767

Research Article

Catalytic Photodegradation of Cyclic Sulfur Compounds in a Model Fuel Using a Bench-scale Falling-film Reactor Irradiated by a Visible Light

Noor Edin. Mousa[1], Seba S. Mohammed[2], Zainab Y. Shnain[1,*], Mohammad F. Abid[3], Khalid A. Sukkar[1], Asawer A. Al-Wasiti[1]

[1]Chemical Engineering Department, University of Technology, Baghdad, Iraq.
[2]Institute of Northern Technical University, Department of Chemical and Oil Industries, Mosul, Iraq.
[3]Department of Oil and Gas Refining Engineering, Al-Turath University College, Al-Mansour Quarter, Baghdad, Iraq.

Received: 15th September 2022; Revised: 31st October 2022; Accepted: 3rd November 2022
Available online: 8th November 2022; Published regularly: December 2022

Abstract

A homemade N doped-TiO_2 nanoparticle were used to degrade dibenzothiophene (DBT) in a model fuel flowing on a bench-scale glass-made falling film reactor irradiated by a xenon lamp that emitted visible light. The photocatalyst was immobilized on the glass sheet. EDS, SEM, and FT-IR techniques were utilized to identify the morphology of the N doped-TiO_2 nanoparticles. Different operating parameters (*e.g.*, N loading (0, 4, 5, and 6 wt%), light intensity (20, 40, and 60 W/m^2), and pH (4, 7, and 10)) were investigated for their effect on the DBT degradation. The effect of the N loading on the wettability of the nano-TiO_2 particles was also investigated. Experimental results revealed that the N loading did not affect the wettability characteristics of the nano TiO_2 particles. Moreover, results showed that DBT conversion positively depends on N loading, light intensity (hv), and pH increase. The estimated optimal operating parameters were 5 wt% N loading, pH = 10, and hv = 40 W/m^2 to ensure the best photooxidation efficiency of 91.4% after 120 min of operation. The outcomes of the present work confirmed the effective efficiency of the N-doped TiO_2 nanoparticles irradiated by visible light for DBT degradation.

Keywords: dibenzothiophene; N-doped-TiO_2; nanoparticles; wettability; photodegradation

How to Cite: N.E. Mousa, S.S. Mohammed, Z.Y. Shnain, M.F. Abid, K.A. Sukkar, A.A. Al-Wasiti (2022). Catalytic Photodegradation of Cyclic Sulfur Compounds in a Model Fuel Using a Bench-scale Falling-film Reactor Irradiated by a Visible Light. *Bulletin of Chemical Reaction Engineering & Catalysis*, 17(4), 755-767 (doi: 10.9767/bcrec.17.4.15838.755-767)

Permalink/DOI: https://doi.org/10.9767/bcrec.17.4.15838.755-767

1. Introduction

The desulfurization of petroleum distillates has become the researcher's interest due to the benzothiophene, dibenzothiophene, and their derivatives existing in crude oil are the reason for many environmental problems like acid rain deactivates of the catalyst and corrodes equipment in refining industries. These sulfur compounds are refractory and hard to be degraded using classical hydrodesulfurization (HDS) due because of their steric retarding [1]. However, there are other processes examined for fuel desulfurization under ambient conditions like; biodesulfurization [2], extractive desulfurization [3], and adsorptive desulfurization [4,5], oxidative desulfurization [6,7] and photooxidation [8,9]. Removal of sulfur by photocatalysis is a successful technique for degrading the S-compounds to polar compounds that easily be

* Corresponding Author.
Email: asawer.a.alwasiti@uotechnology.edu.iq (A.A. Al-Wasiti)

removed by physical processes. A Photocatalysis is conducted under the combined action of light and catalyst. This technique has many virtues inclusive of the protection of the environment, and the total removal of contaminants.

Researchers frequently employ photocatalytic degradation as an efficient method for the degradation of sulfur compounds. Different semiconductors have been utilized as photocatalysts for photocatalytic desulfurization up until now. Although these photocatalysts have many advantages, including extremely high porosity, high specific surface area, and extremely low density, some limitations, including the high recombination efficiency of the photogenerated electron-hole pairs, low visible-light absorption, ease of agglomeration, collecting, and their challenging removal from the treated waste, are rather complex and restrict the use of photocatalysis in industries. The light energy required to generate (e^-–h^+) pairs on TiO_2, is proportional to its bandgap energy [10,11]. The new contribution of this research, a novel nanohybrid of nitrogen-doped-TiO_2 nanoparticles with various nitrogen loading ratios (from 0 to 6 wt%), has been synthesized as a visible-light unique photocatalyst immobilized on a transparent glass sheet and irradiated by an artificial visible light (*e.g.*, a Xenon lamp) for dibenzothiophene (DBT) removal from model fuel. This research was carried out to overcome the band gap (~3.2 eV) for the pure anatase phase of TiO_2, and has been carried out to shift the excitation of TiO_2 nanoparticles into the visible region by decreasing the band gap [12-14], thus enabling the use of sunlight for photo-catalysis. Doping TiO_2 with transition metals, such as Cu, Cr, Fe, *etc*. [15,16], and nonmetals, such as C, N, and S [17], was attempted. Mittal *et al*. [18] reported that doping semiconductors with non-metals is a promising, efficient, and economic technique to utilize visible light to degrade organic pollutants.

In this work, the synthesized nitrogen-doped- TiO_2 nanoparticles were immobilized on a transparent glass sheet and irradiated by an artificial visible light (*e.g.*, a Xenon lamp) to degrade DBT. Different operating parameters such as light intensity, wt% nitrogen, and pH were investigated for their effect on the removal efficiency of DBT.

2. Mechanism of Photocatalytic

All semiconductors have two energy bands in their framework, a low-energy band (valence band: VB) and a high-energy band (conduction band: CB). When a photocatalyst surface is irradiated by UV or visible light (photon energy ($h\nu$)) that equivalents or more than the band-gap energy of the photocatalyst to initiate the photocatalysis process [19-20], electrons will be agitated and, as a result of this agitation, the formation of electrons (e-CB) in the conduction band and holes (VB $h\nu$) in the valence band as in Equation (1).

$$\text{N-TiO}_2 + h\nu_{\text{(visible light)}} \rightarrow h^+_{\text{(VB)}} + e^-_{\text{(CB)}} \quad (1)$$

Usually, the generated holes have a strong oxidation capacity, which can react easily with the molecules of water to generate hydroxyl radicals (OH•) as in Equation (2).

$$h^+_{\text{(VB)}} + \text{OH}^- \rightarrow \cdot\text{OH} \quad (2)$$

While the exited electrons in the conduction band have a strong reduction capacity, which can react with molecular oxygen dissolved inside water or O_2 adsorbed on the photocatalyst surface to form superoxide radical anions ($O_2^{\bullet -}$) or hydroperoxide radicals (HO_2), as in Equations (3)-(6):

$$e^-_{\text{(CB)}} + O_2 \rightarrow O_2^{\bullet -} \quad (3)$$
$$O_2^{\bullet -} + h^+ \rightarrow HO_2^{\bullet} \quad (4)$$
$$2HO_2^{\bullet} \rightarrow H_2O_2 + O_2 \quad (5)$$
$$e^-_{\text{(CB)}} + H_2O_{2\,\text{(ads.)}} \rightarrow \text{OH}^- + \cdot\text{OH} \quad (6)$$

The species •OH, H^+, $O_2^{\bullet -}$, and $HO_2^{\bullet}$ are very reactive and can oxidize organic compounds, initiating subsequent degradation processes, as in Equation (7):

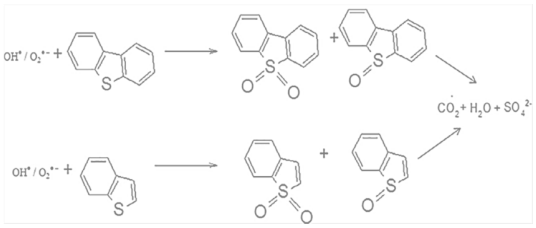

(7)

3. Materials and Methods

3.1 Chemicals and Reagents

Titanium(IV) isopropoxide ($Ti[OCH(CH_3)_2]_4$) with a purity of 98.6% was obtained from Sigma Aldrich in India. Nitric acid (HNO_3), 65% purity, was supplied by Thomas Baker, India. Hydrochloric acid (HCl), 37% purity, was supplied by Merck India. Sodium hydroxide (NaOH) of 99% purity was supplied by Chem-Lab NV Belguim, and H_2O_2 with a 30% concentration was obtained from BDH-Analar-England. DBT and n-octane (C_8H_{18}) were pur-

chased from Merck. Deionized water (DI) was purchased from the local market. All the chemicals received were used without any further treatment.

3.2 Methods

3.2.1 Catalyst synthesis

To synthesize N doped-TiO_2, 4 mL of titanium isopropoxide (TTIP) were mixed with 100 ml of distilled water for 10 min using a magnetic stirrer (Model SH-3, China). After that, 40 mL of HNO_3 (65%) was put into the suspension and mixed until it turned into a transparent solution. Then, 200 mL of NH_4OH (25%) was slowly added to the solution while mixing for 60 min. The precipitate obtained was filtered under a vacuum and dehydrated at 40 °C for 24 h. Then the N-doped-TiO_2 was calcined at 450 °C for a period of 120 min.

3.2.2 Experimental setup

Figure 1(a) and (b) show the schematic and photographic view of the reaction system, respectively. The photocatalytic reactor was designed and hand- made to operate as a batch process. The system consists of a falling-film type photoreactor of dimension 10 cm width x 16 cm long, a wastewater preparation vessel of 1-L, a circulation dosing-type pump (Type DDE 6-10 B-PVC/V/C-X-31I001FG, PolyPump Limited, UK), and a control panel. The photoreactor was mounted on a fixed platform tilted 37° (local latitude). It was made up of a flat-plate colorless glass. The base of the reactor was made of aluminum. Three 8 W Xenon lamps have been used with an intensity of 20 W/m^2 for each lamp. The lamps were mounted 15 cm high perpendicularly to the glass photoreactor. The dosing pump was utilized to charge the wastewater from the vessel to the reactor through a flow meter that was previously calibrated. The wastewater was trickling from a pierced pipe, with ten 0.1 mm holes, from the top of the reactor. The synthetic wastewater was prepared and added to the vessel. A thermocouple was placed into the wastewater preparation vessel to monitor the reaction temperature. A 6-mm PVC tube was immersed in the vessel and was used for oil-free air to obtain homogeneous conditions in the vessel. Immobilization of the prepared N- doped TiO_2 for each wt% of N was conducted according to the method of [21].

3.2.3. Experimental design

Design-Expert software has been used to design the experiments and optimize and evaluate the system. The Response Surface Method was chosen for this study since it is a well-known statistical approach for designing experiments. Design analysis and mathematical modeling by using ANOVA provide Normal Probability Plots, Actual vs. Predicted Plots, and model-graphs, including Interaction. A four-factorial (four-level) central composite design (CCD) was used to investigate the effects of the independent variables, pH, N loading, and light intensity. These factors are shown in Table 1.

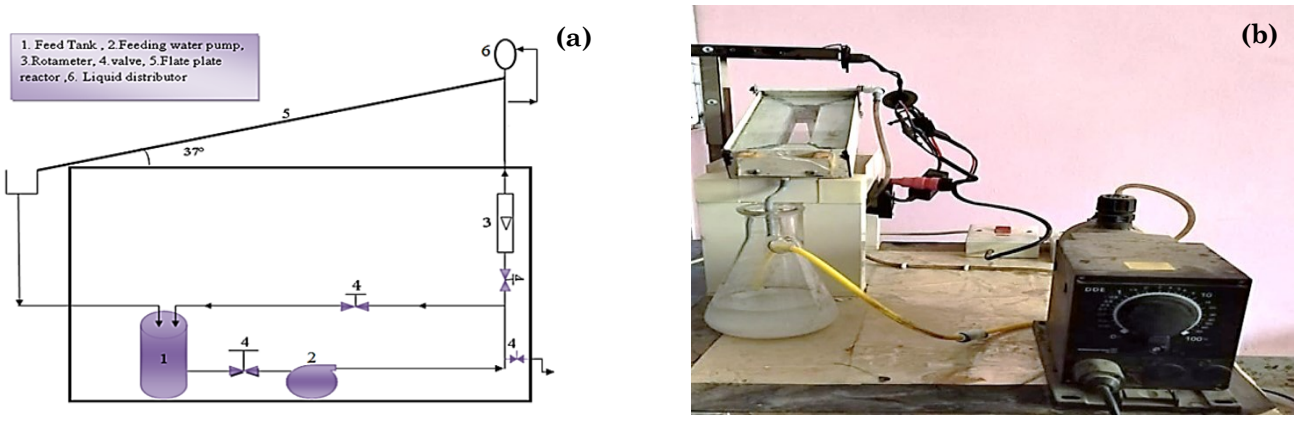

Figure 1. Schematic (a) and (b) photographic image of the photocatalytic reactor.

Table 1. Independent variable levels and experimental range.

Factor	Name	Units	Type	Minimum	Maximum
A	N loading	wt%	Numeric	0.0000	6.00
B	Light intensity	W/m^2	Numeric	20.00	60.00
C	PH		Numeric	4.00	10.00

The optimum conditions to obtain a maximum percentage of DBT removal were obtained as 91.4%, under the optimum pH = 10, light intensity = 40 W/m^2), and N-loading = 5 wt%. The experimental DBT removal at the optimum condition was close to predicate values, where R^2 = 0.988.

3.2.4. Analysis techniques

The prepared N doped-TiO_2 was characterized using an Energy Dispersive Spectroscopy (EDX-7000P, Shimadzu, Japan), SEM- Model: Inspect 50S, FEI-USA, Fourier transform infrared spectroscopy (Model: The Spectrum Two N system, high-performance FT-NIR, Perkin Elmer) was utilized to characterize the functional groups of the synthesized photocatalyst. The suspension was circulated for about 2 h without illumination and then irradiated under the xenon lamp. The instantaneous loading of DBT was estimated by the Shimadzu UV-vis spectrophotometer (1100 UV-Vis spectrophotometer, China). The contact angle meter model (CAM 110-Taiwan) was utilized to measure the water contact angle (WCA). The percentage degradation (*%R*) of DBT was calculated by Equation (8):

$$Percentage\ degradation\ (\%R) = \frac{C_0 - C_{(t)}}{C_0} \times 100 \quad (8)$$

where, C_0 and $C_{(t)}$ are the initial and instantaneous concentrations of DBT (ppm), respectively. A series of (DBT/n-octane) into the N doped-TiO_2 suspension at concentrations of 0.5, 2, 8, 10, 20, 30, 40, 60, and 75 ppm are used to generate a calibration plot, utilizing the UV-Vis spectrophotometer at 325 nm, as shown in Figure 2.

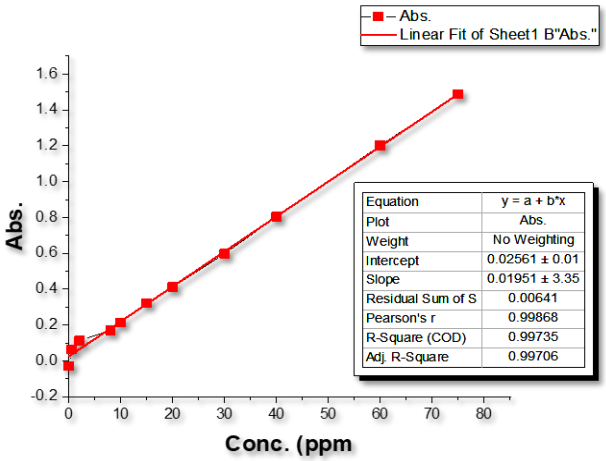

Figure 2. Calibration curve of DBT.

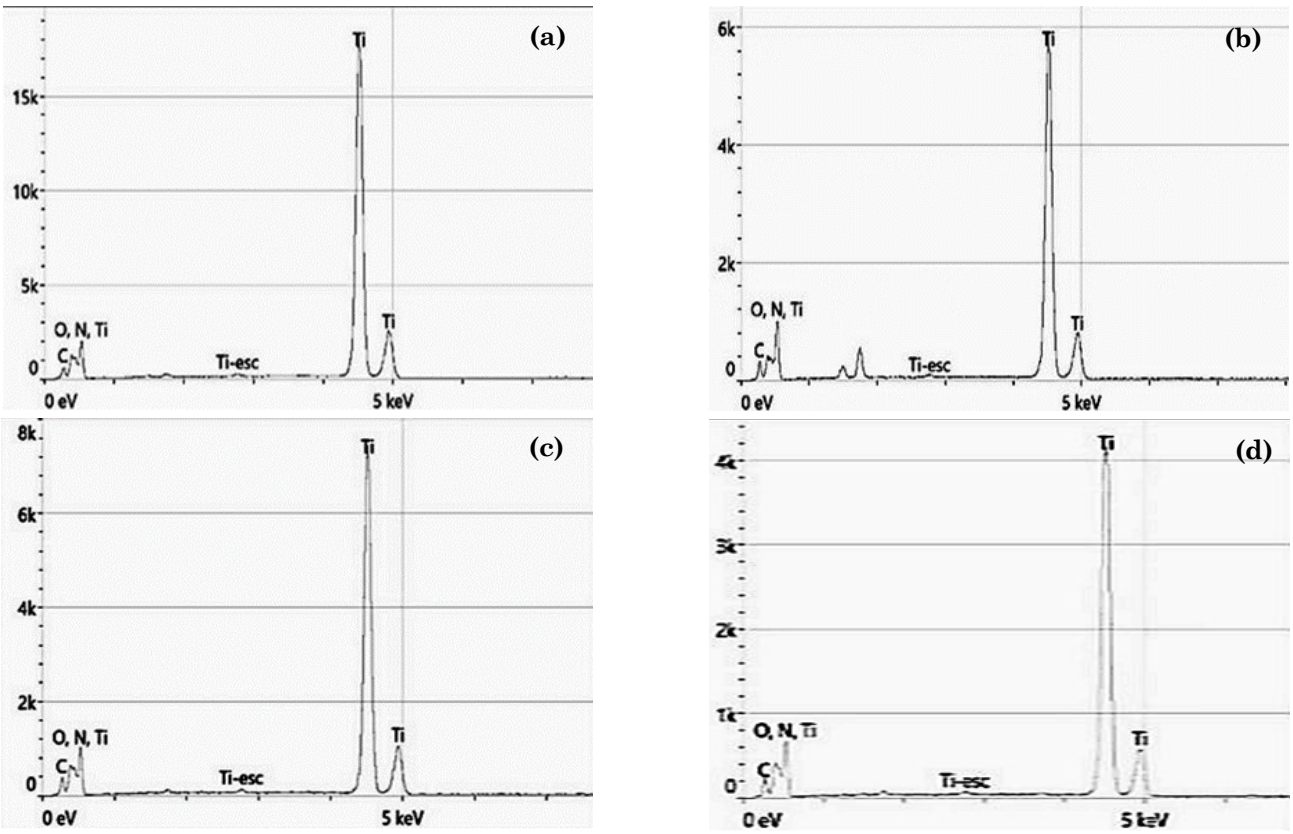

Figure 3. EDS images of N doped-TiO_2 for (a) 0 %N; (b) 4 %N; (c) 5 %N; and (d) 6 %N.

4. Results and Discussion

4.1 Catalyst Identification

4.1.1 EDS analysis

Figure 3 (a, b, c, and d) depicts the EDS images of N doped-TiO_2 Nps for 0, 4, 5, and 6 wt% N respectively. These images have been analyzed for the elemental compositions following the method used by Wassilkowska *et al*. [20]. The EDS data of N-TiO_2 samples (Figure 3) depicts a peak of about 0.4 and 0.5 keV and else keen peaks appear at 4.5 and 4.9 keV for Ti [22]. The peaks resulting in N and O are obviously special at 0.3 and 0.6 keV, respectively. These outcomes emphasize that Ti, O, and N occur in the catalyst framework. Results of the concentration measurement of the elements for the N doped-TiO_2 samples are listed in (Table 2). The list of the characterized elements is generated automatically on the base of all the peaks labeled as 'characterized' by Noran System 7 (NSS) analytical software, or labeled manually (e.g. nominating the choice 'peak-off' of carbon).

4.1.2 SEM analysis

Figure 4 displays a contrast among SEM images of undoped-TiO_2 (a) TiO_2 N4% (b) TiO_2 N5% (c), and TiO_2 N6% (d), respectively. The analysis of specimens demonstrates that the

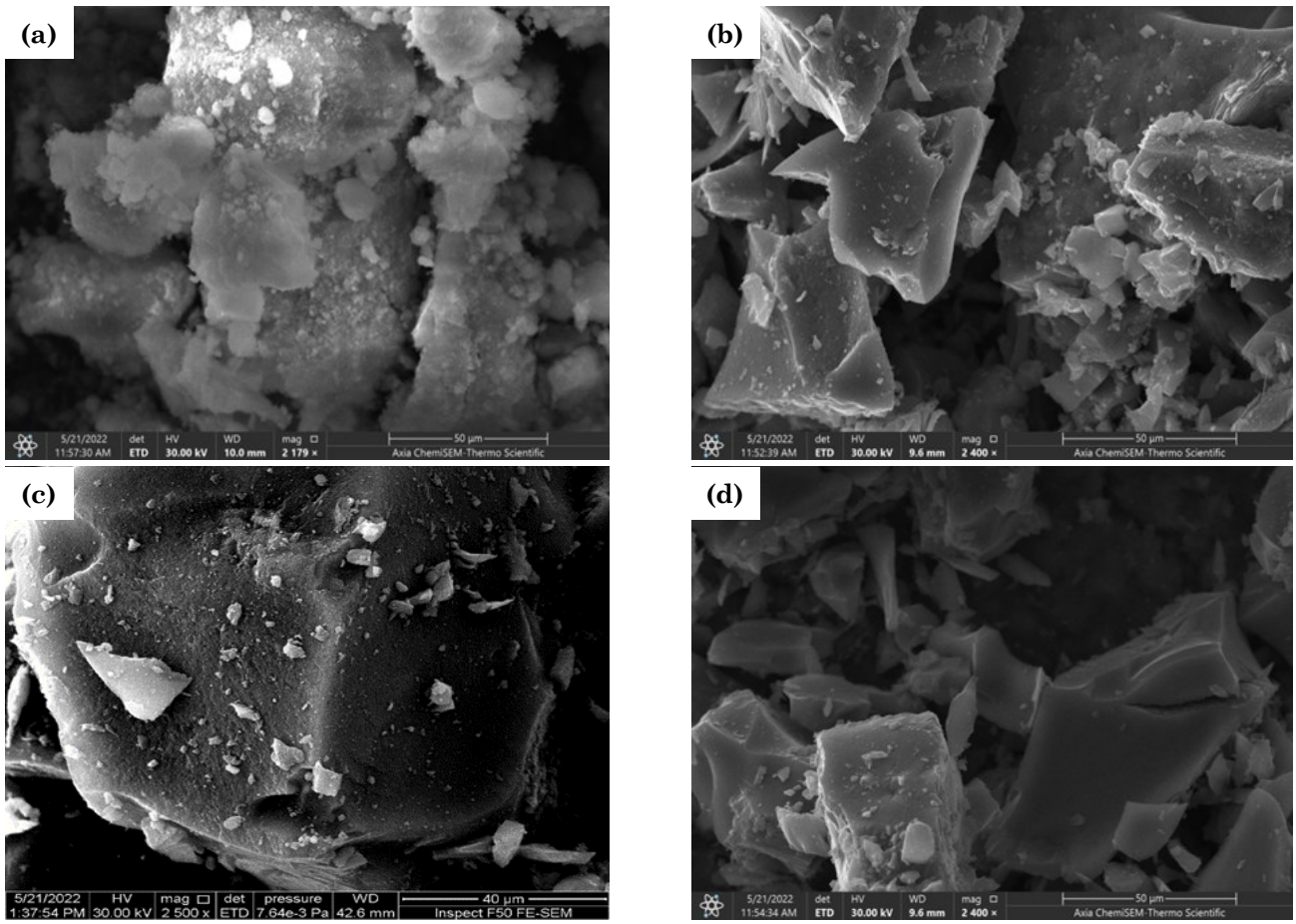

Figure 4. SEM images of various wt%N loading onto TiO_2 ((a) undoped-TiO_2, (b) TiO_2 N4%, (c) TiO_2 N5%, and (d) TiO_2 N6%).

Table 2. Analysis of the EDS images.

Element	0 wt% N		4 wt% N		5 wt% N		6 wt% N	
	Atomic (%)	Weight (%)	Atomic (%)	Weight (%)	Atomic (%)	Weight (%)	Atomic (%)	Weight (%)
C	10.1	5.1	7.6	3.7	9.1	4.7	8.2	4.5
N	0.1	0.0	7.5	4.3	8.5	5.1	9.0	5.7
O	64.0	43.0	57.3	37.7	58.1	40.1	61.5	44.2
Ti	25.8	51.9	27.6	54.3	24.2	50.1	21.2	45.6

existence of N alters the surface characteristics (Figure 4). Undoped-TiO_2 grains have rounded forms and take sponge-like clusters, while N-doped-TiO_2 takes shape lamellar isolated clusters. The change in the quantity of N ions within the crystal framework does not suggest more variation in surface characteristics. The cause is that the form stability of TiO_2 Nps highly relies on surface chemistry, and the preparation conditions do a major function. Referring to theoretical models [23], in the status of hydrogenated and hydrated surfaces, there were negligible changes in the form of TiO_2 Nps with surface chemistry; but, in the situation of hydrogen-poor and oxygenated surfaces, nanocrystals of both polymorphs were elongated, and this could result in the forming of lamellar groups. All images (*i.e.*, b, c, and d) show a good dispersion of N-atoms onto TiO_2 confirming a well-established preparation method.

4.1.3 XRD analysis

X-ray powder diffraction (XRD) analysis was carried out with a Rigaku D/max III apparatus using Cu-Ka radiation (λ = 0.15406 nm), operated at 40 kV and 30 mA. TiO_2 usually exists in two main crystallographic form, anatase (A) and rutile (R). The XRD peaks at 2θ = 25.3° (1 0 1) and 2θ = 27.4° (1 1 0) are often taken as the characteristic peaks of anatase and rutile crystal phase, respectively. The patterns obtained by diffraction analysis are depicted in Figure 5. It can be observed from the plot that the prepared sample is crystalline in nature and there is no extra peak formed in the nitrogen doped samples. Further in the prepared sample the peaks are located at 24.6˚, 37.3°, 47.3°, 53.7°, 62.2° indexed with Miller indices as (101), (004), (200), (105), and (213) mainly associated with anatase phase according to JCPDS card file 21-1272. The average crystallite size of prepared Nano-powders was calculated from full width at half maximum (FWHM) values corresponding to diffraction peaks by using Debye-Scherrer formula as follows (Equation (9)) [24]:

$$D = \frac{K\lambda}{\beta \cos\theta} \tag{9}$$

where, D is the crystallite size, λ is the wavelength of the X-ray radiation (in our test, λ = 0.15406 nm), K is usually taken as 0.89, and β is the full width at half-maximum height of the main intensity peak after subtraction of the equipment broadening. Meanwhile, the percentage of anatase in the TiO_2 samples can also be estimated from the respective integrated characteristic XRD peak intensities using the quality factor ratio of anatase to rutile (1.265). X-Ray wavelength, b is full width at half maximum (FWHM) and θ is the Bragg's angle. The calculated average crystallite sizes for N5%TiO_2 sample are reported in Table 1.

4.1.4 FTIR analysis

Figure 6(a) plots the FTIR images of TiO_2, the absorption peak seen in 3000-3500 cm^{-1} is specified to the stretching forms of OH bonds

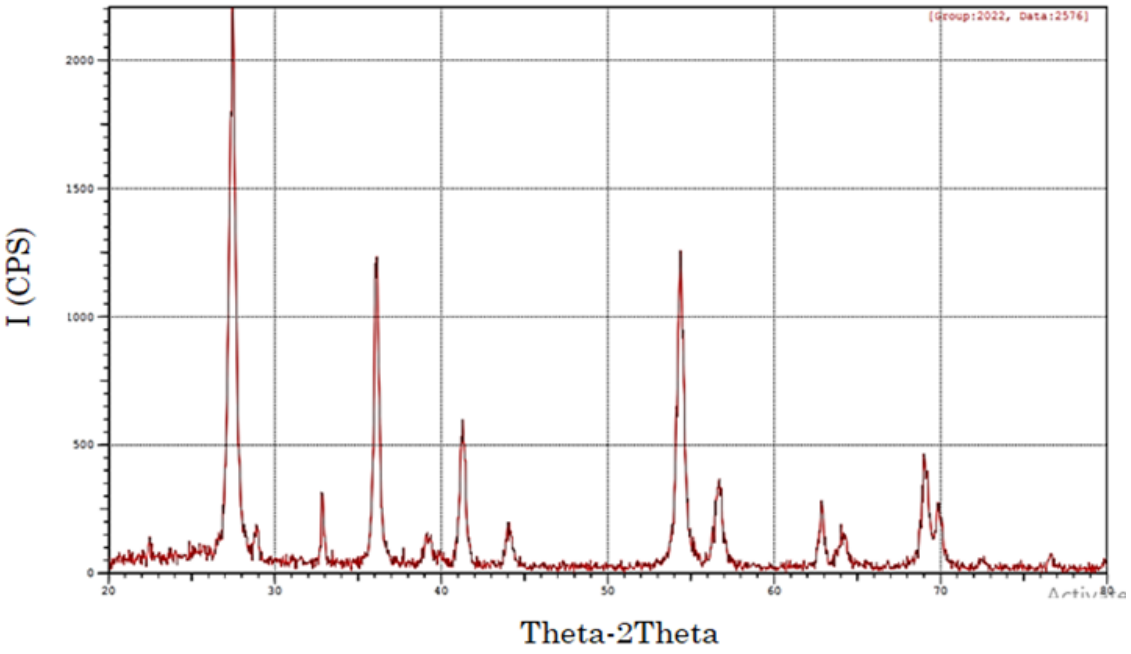

Figure 5. XRD images of 5 wt%N loading onto TiO_2.

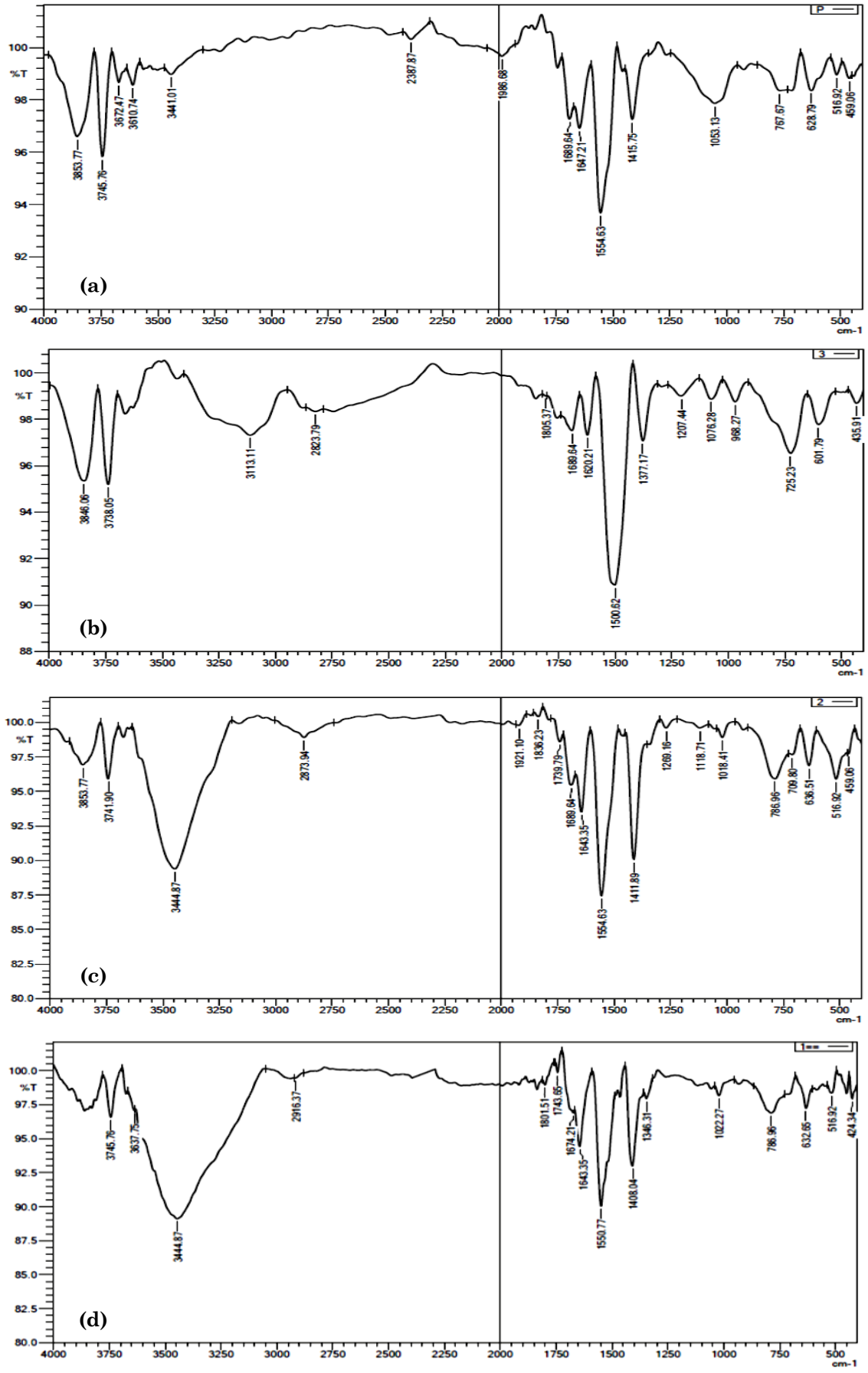

Figure 6. FT-IR spectra of doped-TiO_2 for (a) undoped-TiO_2, (b) TiO_2 N4%, (c) TiO_2 N5%, and (d) TiO_2 N6%.

and linked to free H_2O molecules. The peak about 558 cm^{-1}, is due to the stretching vibration of Ti–O bonds. The peak at 1626 cm^{-1} was due to the sorbed H_2O. Figures 6(b), (c), and (d) show the spectra of N-TiO_2 powders from different mole ratios of HNO_3, respectively. The FTIR spectra of the N-TiO_2 catalyst display a high peak at 3000-3700 cm^{-1} and a tight band at 1628 cm^{-1} that is allocated to the O–H stretching and H–O–H bending vibrations of sorbed H_2O molecules. The peaks shown in 1384, 1163, and 1019 cm^{-1} are ideal for N–O stretching and O–N–O bending vibrations, respectively [24]. Moreover, the peak at 514 cm^{-1} for N-TiO_2 is due to Ti–O–Ti bending vibrations, being red-shifted in comparison to the peak for TiO_2 at 539 cm^{-1}, and the peak at 653-550 cm^{-1} is related to the Ti–O stretching vibration [25]. The small absorption peak at 1050 m^{-1} for the N–Ti–O bond was seen for all the prepared N-doped TiO_2 samples, assuring the N combination into TiO_2 [26].

4.2 Effect of Operating Parameters on DBT Oxidation

4.2.1 Effect of N loading on TiO_2 contact angle

It is well-known that the degree of wettability of TiO_2 Nps enhances the surface photocatalytic activity [27]. In the present work, the effect of N loading on the hydrophilicity of TiO_2 Nps was studied. The contact angle meter model (CAM 110-Taiwan) was utilized to measure the water contact angle (WCA); a 5 µL DI water drop was dripped on the catalyst particle. Figure 7 (a, b, c, and d) represents the computer images of contact angles obtained for water

Table 3. Effect of N loading on catalyst´s contact angle.

Item	wt% N loading	Water contact angle (°)
1	0	13.06
2	4	28.22
3	5	46.43
4	6	51.32

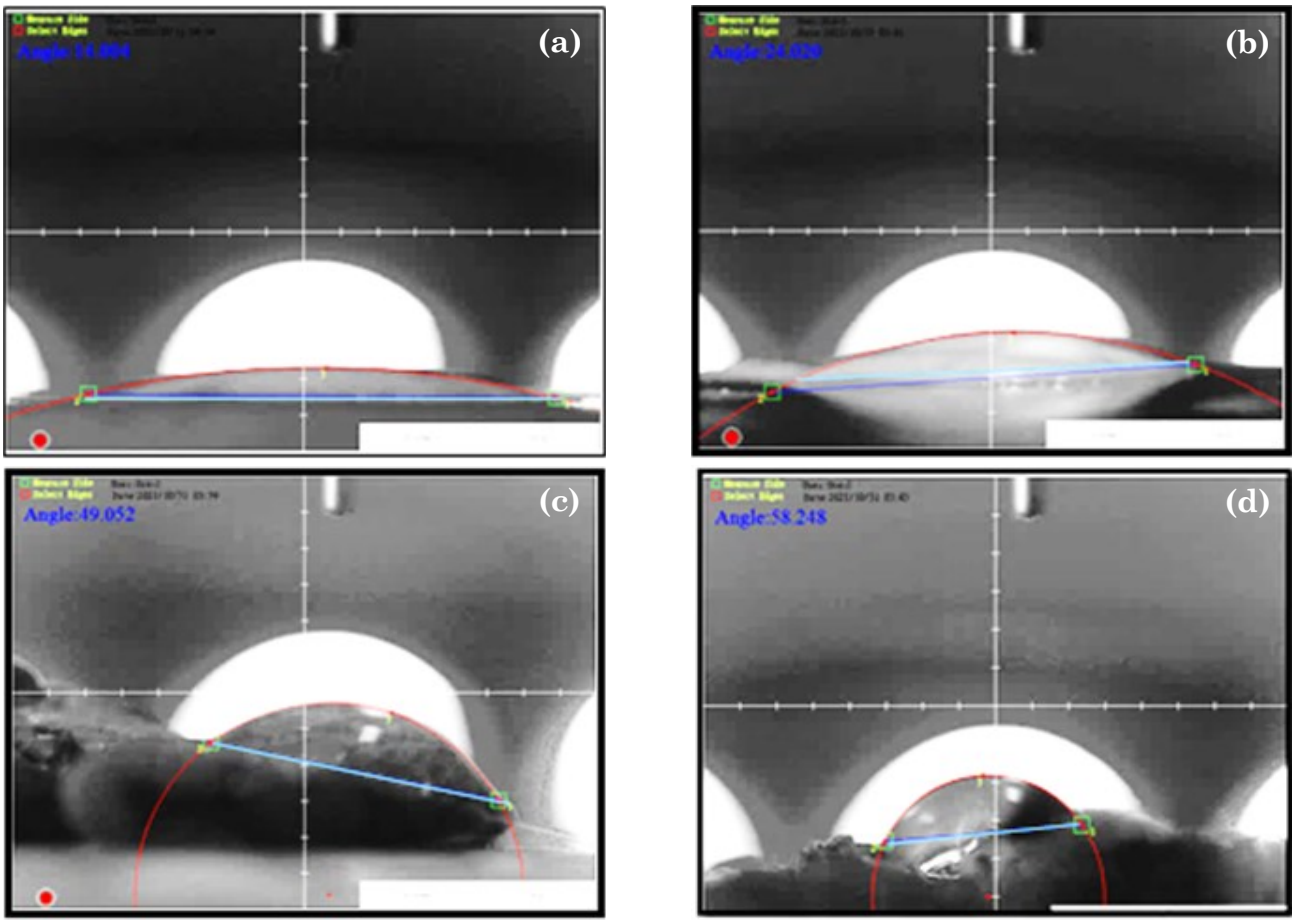

Figure 7. Images of contact angles for (a) N-free TiO_2, (b) 4 wt% N-TiO_2, (c) 5 wt% N-TiO_2, and (d) 6 wt% N-TiO_2.

sprayed on various N-loaded specimens. Generally, the literature indicates that if the WCA is < 90°, the sample surface is counted as hydrophilic. If the WCA is > 90°, the sample surface is hydrophobic [28]. Table 3 revealed that catalysts of N loading (0, 4, 5, and 6 wt%) have contact angles of 13.06, 28.22, 46.43, and 51.32 degrees, respectively, indicating that the N loading over the specimen surface does not affect the hydrophilicity that helps remove solid pollutants that adhere to surfaces by washing. The present trend of results is well agreed with previously published data [29,30].

5.2.2 Effect of illumination time and Nitrogen loading

Figure 8 illustrates the change of DBT removal against illumination time for different wt%N onto TiO_2 nanoparticles at pH=10 and a xenon lamp intensity of 60 W/m². The photo-degradation time was estimated after the sorption of DBT onto the TiO_2 Nps had approached equilibrium in the dark. As observed in Figure 8 when the time of illumination was increased to 120 min the degradation of DBT increased as a result of this and the degradation was stable after this time. This trend may be due to that as the illumination time is raised, more free radicals are generated and boosted the degradation of DBT till the loading of DBT onto the TiO_2 surface is decreased. Moreover, as observed in Figure 8, the outcomes reveal that the used N-source shows higher photocatalytic effectiveness of prepared N-TiO_2 in the degradation process. All N-TiO_2 specimens offer the best photo-activity in comparison to undoped-TiO_2. It is seen in Figure 8 that after a xenon light irradiation of 20 min, the percentage degradation of DBT was 33.3, 51.7, 62.4, and 66.3% when N content increased from 0, 4, 5, and 6%, respectively. Moreover, after xenon lamp illumination for 130 min, the results marked that boosting the N loading from 0, 4, 5, and 6 wt% increased the desulfurization rate from 63.5, 83.3, 90.7, and 91.5%, respectively. The present outcomes agree with the previously published data of [31,32].

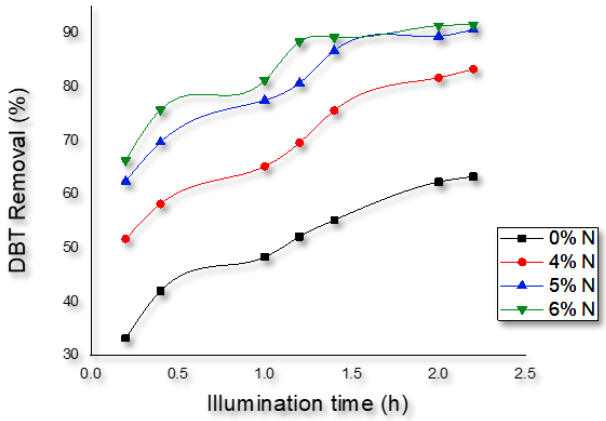

Figure 8. Variation of DBT removal against illumination time for different wt%N onto TiO_2 nanoparticles at pH=10, and a light intensity of 60 W/m².

5.2.3 Influence of light intensity

Figure 9 plots the influence of light illumination on % DBT degradation for different N wt% loading and a pH = 10. As can be observed in Figure 9 that after 130 min of illumination as light flux was enhanced from 20, 40, and 60 W/m² the %DBT degradation boosted from 75.6, 88.2, and 92.2 % correspondingly for N loading of 6 wt%. The plot points out a positive relationship between xenon illumination and DBT removal. This relationship occurs due to

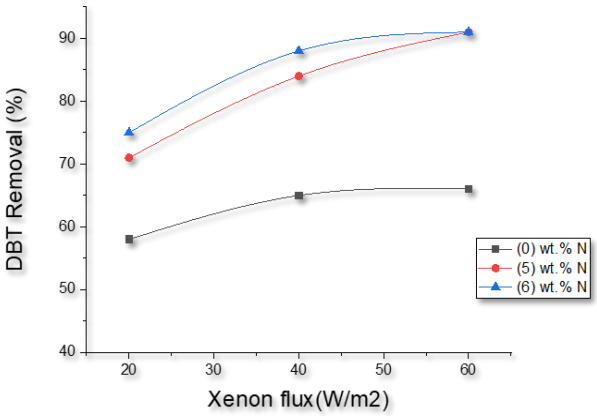

Figure 9. effect of light intensity on %DBT degradation for different N wt% loading and a pH = 10.

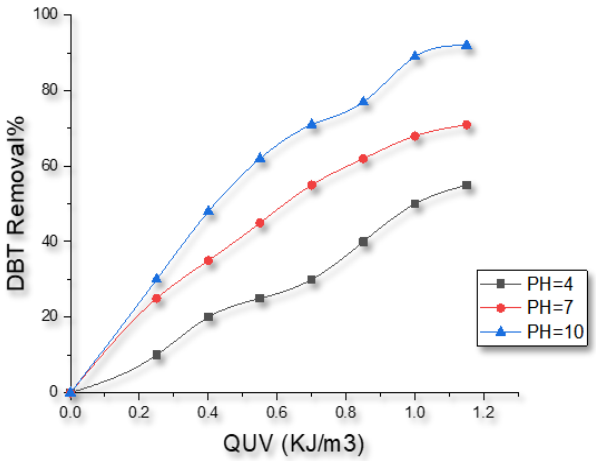

Figure 10. Variation of DBT removal versus irradiation energy accumulated in wastewater for different pH at irradiation flux = 60 W/m².

that enhancing light illumination on a semiconductor surface boosting the rate at which the (e^-–h^+) pairs are formed then increasing the generation rate of •OH radicals resulting in more oxidation of DBT. This link is also obvious in the data from [34-36]. Furthermore, the behavior of illumination against DBT degradation in Figure 9 shows a linear relation before the parting point (*i.e.*, 40 W/m^2, 88.1%), and a nonlinear relation after this point [37,38]. This could be due to that in the linear region, e^-–h^+ pairs are loaded by reactions with species (*e.g.*, OH^-) on the TiO_2 surface quicker than by rejoining with excited electrons; on other hand, in the nonlinear system, h^+ are filled by rejoining at a quicker rate than by reaction with other species this commentary be in agreement with the data of Jacoby *et al*. [37]. Moreover, Figure 9 shows that for a loading of 5 N wt% as light irradiance boosted from 20, 40, and 60 W/m^2 the %DBT degradation enhanced from 70.6, 82.2, and 91.2% making the 6 wt% N has an average increase in %DBT removal of only 3.3%.

4.2.4 Effect of pH

Figure 10 plots the variation of DBT removal versus irradiation energy accumulated in the wastewater for different pH (4-10) after 130 min. The accumulated solar energy per unit volume of polluted liquid ($Q_{,n}$) in the illuminated reactor for the n^{th} sample was calculated by Equation (10) [39].

$$Q_{,n} = Q_{,n-1} + \Delta t_n \times UV_{GN} \times \frac{A}{V} \quad (10)$$

where, Δt is time difference between two successive samples (~20 min), A is irradiated area of the reactor (W×L) cm^2, V is volume of polluted liquid in the experimental setup = 0.5 L, n is number of samples, and UV_{GN} is the average global energy of illumination = 60 W/m^2. In Figure 10, the initial pH of polluted liquid was changed from 4 to 10 with other operating parameters hold at (C_{DBT} = 50 mg/L, $C_{N\text{-}TiO2}$ = 400 mg/L, Q_{sw} = 1.0 L/min). In Figure 10, it is seen that after 130 min of the xenon lamp irradiance, the values of %R reached 55, 78, and 92.5 when the initial pH of the solution was 4, 7, and 10 respectively. This trend may be due to the surface charge of TiO_2. In a solution of pH<7, N-TiO_2 acquires a negative charge resulting in attraction forces between the TiO_2 surface and the DBT ions in the solution enhancing the adsorption of thes1e ions onto the illuminated surface of N-TiO_2 then boosting the DBT degradation. However, the opposite behavior was observed in the acidic environment. This could be because of the electro-repulsion forces between TiO_2 Nps and DBT cations in the suspension hindering the sorption of cations onto the N-TiO_2. Abid *et al*. [40] presented Equations (11) and (12) showing the variation of the characteristics of TiO_2 surface with the change of pH of the polluted liquid near its pH_{pzc}.

$$TiOH + H^+ \leftrightarrow TiOH_2^+ \quad pH < pH_{pzc} \quad (11)$$
$$TiOH + OH^- \leftrightarrow TiO^- + H_2O \quad pH > pH_{pzc} \quad (12)$$

The aforementioned suggests that pH changes impact the adsorption of DBT cations onto the TiO_2 surface, an essential step for photooxidation to take place. For the prepared N-TiO_2, pH_{pzc} of our synthesized TiO_2 was between 6-6.2. Hence, when the pH of the solution is >6.2 the sorbed ions of DBT onto the TiO_2 begin to enhance because of the increase of TiO-groups on the TiO_2 surface. In our work, %R approached maxima at pH=10. Consequently, the photolysis of DBT attains higher values in alkaline media (*i.e.*, when pH is >7). The present outcomes are well-agreed with the previously published data of Kim [41] who in his experimental work found that the degradation of benzothiophene (BT) in alkaline pH is higher than that in acidic. The author deduced that contest on sorption sites between BT and the (H_2O/OH^-) ratio at different pH was anticipated to affect the rate of reaction, and the mechanism of photodegradation. Moreover, the authors revealed that the increase in the rate of degradation with increasing pH may be due to the increased number of OH^- ions on the surface of TiO_2. Also, Kim *et al*. [42] studied the photodegradation of DBT under various operating parameters. They found that a higher degradation of DBT occurred in the alkaline solution. The authors attributed this behavior to the ionization of DBT which became higher in alkaline solution.

5. Conclusion

Dibenzothiophene existing in diesel is one of the main sulfur-containing organic pollutants in fuel oils and is difficult to be removed by the conventional hydrodesulfurization (HDS) method. In the present research, an environmental friendly technology at ambient conditions was used to remove DBT in a model fuel. A homemade N doped-TiO_2 nanoparticles was prepared and immobilized on a bench-scale glass-made falling film reactor irradiated by a xenon lamp that emitted a visible light. Con-

tact angle measurements indicated that the N loading over the photocatalyst surface did not affect the hydrophilicity of TiO_2. Experimental results revealed that DBT degradation was dependent positively on the N loading, light intensity, and increasing pH. The results of our work confirmed the effective efficiency of the N-doped TiO_2 nanoparticles irradiated by visible light for DBT degradation.

Acknowledgements

The authors are grateful to the Chemical Engineering department, the University of Technology for providing space and facilities. Thanks are also due to the Al-Turath University College for assistance.

Conflict Interest

The authors declare that their present work has no conflict interest with any person or previous published data.

References

[1] Song, C. (2003). An overview of new approaches to deep desulfurization for ultra-clean gasoline, diesel fuel and jet fuel. *Catalysis Today*, 86(1-4), 211-263. DOI: 10.1016/S0920-5861(03)00412-7.

[2] Yu, F., Liu, C., Yuan, B., Xie, P., Xie, C., Yu, S. (2016). Energy-efficient extractive desulfurization of gasoline by polyether-based ionic liquids. *Fuel*, 177, 39-45. DOI: 10.1016/j.fuel.2016.02.063.

[3] Abd El-Aty, D.M., Sif El-Din, O.I., Hassan, S.I., Tawfik, S.M., Hanafi, S. (2009). Evaluation of some organic solvents for refining diesel fuel fraction. *Petroleum Science and Technology*, 27(9), 861-873. DOI: 10.1080/10916460802096279.

[4] Abd El-Aty, D.M., Zaki, T., Tawfik, S.M., El-Dine, O.S., Hassan, S.I., Ahmed, S.H. (2016). Effect of the Synthesis Conditions on The Desulfurization Power of Mesoporous Alumina. *Egyptian Journal of Chemistry*, 59(3), 381-396. DOI: 10.21608/ejchem.2016.1088.

[5] Lee, K.X., Valla, J.A. (2019). Adsorptive desulfurization of liquid hydrocarbons using zeolite-based sorbents: a comprehensive review. *Reaction Chemistry & Engineering*, 4(8), 1357-1386. DOI: 10.1039/C9RE00036D.

[6] Hassan, S.I., El-Din, O.I.S., Tawfik, S.M., Abd El-Aty, D.M. (2013). Solvent extraction of oxidized diesel fuel: Phase equilibrium. *Fuel Processing Technology*, 106, 127-132. DOI: 10.1016/j.fuproc.2012.07.012.

[7] Rezvani, M.A., Asli, M.A., Khandan, S., Mousavi, H., Aghbolagh, Z.S. (2017). Synthesis and characterization of new nanocomposite CTAB-PTA@ CS as an efficient heterogeneous catalyst for oxidative desulphurization of gasoline. *Chemical Engineering Journal*, 312, 243-251. DOI: 10.1016/j.cej.2016.11.137.

[8] Lin, F., Jiang, Z., Tang, N., Zhang, C., Liu, T., Dong, B. (2016). Photocatalytic oxidation of thiophene on RuO2/SO42−TiO2: Insights for cocatalyst and solid-acid. *Applied Catalysis B: Environmental*, 188, 253-258. DOI: 10.1016/j.apcatb.2016.02.016.

[9] Yun, L., Yang, Z., Yu, Z.B., Cai, T., Li, Y., Guo, C., Qi, C., Ren, T. (2017). Synthesis of four-angle star-like CoAl-MMO/BiVO 4 p–n heterojunction and its application in photocatalytic desulfurization. *RSC advances*, 7(41), 25455-25460. DOI: 10.1039/C7RA03012F.

[10] Moctezuma, E., Leyva, E., Aguilar, C.A., Luna, R.A., Montalvo, C. (2012). Photocatalytic degradation of paracetamol: Intermediates and total reaction mechanism. *Journal of Hazardous Materials*, 243, 130-138. DOI: 10.1016/j.jhazmat.2012.10.010.

[11] Zhou, R., Guzman, M.I. (2014). CO2 reduction under periodic illumination of ZnS. *The Journal of Physical Chemistry C*, 118(22), 11649-11656. DOI: 10.1021/jp4126039

[12] Zhang, F., Wang, X., Liu, H., Liu, C., Wan, Y., Long, Y., Cai, Z. (2019). Recent advances and applications of semiconductor photocatalytic technology. *Applied Sciences*, 9(12), 2489. DOI: 10.3390/app9122489.

[13] Khedr, T.M., El-Sheikh, S.M., Hakki, A., Ismail, A.A., Badawy, W.A., Bahnemann, D.W. (2017). Highly active non-metals doped mixed-phase TiO2 for photocatalytic oxidation of ibuprofen under visible light. *Journal of Photochemistry and Photobiology A: Chemistry*, 346, 530-540. DOI: 10.1016/j.jphotochem.2017.07.004.

[14] Al-Nuaim, M.A., Alwasiti, A.A., Shnain, Z.Y. (2022). The photocatalytic process in the treatment of polluted water. *Chemical Papers*, in press. DOI: 10.1007/s11696-022-02468-7.

[15] Abid, M.F. (2015). Desulfurization of gas oil using a solar photocatalytic microreactor. *Energy Procedia*, 74, 663-678. DOI: 10.1016/j.egypro.2015.07.802.

[16] Shafiq, I., Hussain, M., Shafique, S., Rashid, R., Akhter, P., Ahmed, A., ... & Park, Y.K. (2021). Oxidative desulfurization of refinery diesel pool fractions using LaVO4 photocatalyst. *Journal of Industrial and Engineering Chemistry*, 98, 283-288. doi.org/10.1016/j.jiec.2021.03.040.

[17] Shafiq, I., Hussain, M., Shehzad, N., Maafa, I.M., Akhter, P., Shafique, S., ARazzaq, A., Yang, W., Tahir, M., Russo, N. (2019). The effect of crystal facets and induced porosity on the performance of monoclinic BiVO4 for the enhanced visible-light driven photocatalytic abatement of methylene blue. *Journal of Environmental Chemical Engineering*, 7(4), 103265. DOI: 10.1016/j.jece.2019.103265.

[18] Shnian, Z.Y., Abid, M.F., Sukkar, K.A. (2021). Photodegradation of mefenamic acid from wastewater in a continuous flow solar falling film reactor. *Desalination and Water Treatment*, 210, 22-30. DOI: 10.5004/dwt.2021.26581.

[19] Gupta, S.M., Tripathi, M. (2011). A review of TiO2 nanoparticles. *Chinese Science Bulletin*, 56(16), 1639-1657. DOI: 10.1007/s11434-011-4476-1.

[20] Sahu, M., Biswas, P. (2011). Single-step processing of copper-doped titania nanomaterials in a flame aerosol reactor. *Nanoscale Research Letters*, 6(1), 441. DOI: 10.1186/1556-276X-6-441.

[21] Khalilian, H., Behpour, M., Atouf, V., Hosseini, S.N. (2015). Immobilization of S, N-codoped TiO2 nanoparticles on glass beads for photocatalytic degradation of methyl orange by fixed bed photoreactor under visible and sunlight irradiation. *Solar Energy*, 112, 239-245. DOI: 10.1016/j.solener.2014.12.007.

[22] Pelaez, M., Nolan, N.T., Pillai, S.C., Seery, M. K., Falaras, P., Kontos, A.G., Dunlop, P.S.M., Hamilton, J.W.J., Byrne, J.A., O'Shea, K., Entezari, M.H., Dionysiou, D.D. (2012). A review on the visible light active titanium dioxide photocatalysts for environmental applications. *Applied Catalysis B: Environmental*, 125, 331-349. DOI: 10.1016/j.apcatb.2012.05.036

[23] Raorane, D.V., Chavan, P.S., Pednekar, S.R., Chaughule, R.S. (2017). Green and rapid synthesis of copper-doped TiO2 nanoparticles with increased photocatalytic activity. *Advances in Chemical Science*, 6, 13-20. DOI: 10.14355/sepacs.2017.06.002

[24] Khedr, T.M., El-Sheikh, S.M., Hakki, A., Ismail, A.A., Badawy, W.A., Bahnemann, D.W. (2017). Highly active non-metals doped mixed-phase TiO2 for photocatalytic oxidation of ibuprofen under visible light. *Journal of Photochemistry and Photobiology A: Chemistry*, 346, 530-540. DOI: 10.1016/j.jphotochem.2017.07.004.

[25] Barkul, R.P., Koli, V.B., Shewale, V.B., Patil, M.K., Delekar, S.D. (2016). Visible active nanocrystalline N-doped anatase TiO2 particles for photocatalytic mineralization studies. *Materials Chemistry and Physics*, 173, 42-51. DOI: 10.1016/j.matchemphys.2016.01.035.

[26] Wassilkowska, A., Czaplicka-Kotas, A., Bielski, A., Zielina, M. (2014). An analysis of the elemental composition of micro-samples using EDS technique. *Czasopismo Techniczne. Chemia*, 111(1), 133-148. DOI: 10.4467/2353737XCT.14.283.3371.

[27] Abid, M.F., Hamiedi, S.T., Ibrahim, S.I., Al-Nasri, S.K. (2018). Removal of toxic organic compounds from synthetic wastewater by a solar photocatalysis system. *Desalination and Water Treatment*, 105, 119-125. DOI: 10.5004/dwt.2018.22017.

[28] Fadhil, M. (2012). Hydrodynamic Characteristics Effect of Foam Control in a Three-Phase Fluidized Bed Column. *Journal of Petroleum Research and Studies*, 3(2). E158-E185. DOI: 10.52716/jprs.v3i2.84.

[29] Garlisi, C., Lai, C.Y., George, L., Chiesa, M., Palmisano, G. (2018). Relating photoelectrochemistry and wettability of sputtered Cu- and N-doped TiO2 thin films via an integrated approach. *The Journal of Physical Chemistry C*, 122(23), 12369-12376. DOI: 10.1021/acs.jpcc.8b03650.

[30] Sun, Z., Pichugin, V.F., Evdokimov, K.E., Konishchev, M.E., Syrtanov, M.S., Kudiiarov, V.N., Li, K., Tverdokhlebov, S.I. (2020). Effect of nitrogen-doping and post annealing on wettability and band gap energy of TiO2 thin film. *Applied Surface Science*, 500, 144048. DOI: 10.1016/j.apsusc.2019.144048.

[31] Faghihian, H., Naeemi, S. (2013). Application of a novel nanocomposite for desulfurization of a typical organo sulfur compound. *Iranian Journal of Chemistry and Chemical Engineering (IJCCE)*, 32(3), 9-15. DOI: 10.30492/ijcce.2013.5737.

[32] Kim, I. K. (2014). Degradation of a Refractory Organic Contaminant by Photocatalytic Systems. *Journal of Power System Engineering*, 18(6), 133-139. DOI: 10.9726/kspse.2014.18.6.133.

[33] Hüsken, G., Hunger, M., Brouwers, H.J.H. (2009). Experimental study of photocatalytic concrete products for air purification. *Building and Environment*, 44(12), 2463-2474. DOI: 10.1016/j.buildenv.2009.04.010.

[34] Al-Nuaim, M.A., Alwasiti, A.A., Shnain, Z.Y., AL-Shalal, A.K. (2022). The Combined Effect of Bubble and Photo Catalysis Technology in BTEX Removal from Produced Water. *Bulletin of Chemical Reaction Engineering & Catalysis*, 17(3), 577-589. DOI: 10.9767/bcrec.17.3.15367.577-589.

[35] Alwasiti, A.A., Shnain, Z.Y., Abid, M.F., Abdul Razak, A.A., Abdulhussein, B.A., Mahdi, G.S. (2021). Experimental and numerical study on the degradation of mefenamic acid in a synthetic wastewater. *IOP Conference Series: Earth and Environmental Science*, 779, 012073. DOI: 10.1088/1755-1315/779/1/012073.

[36] Hüsken, G., Hunger, M., Brouwers, H.J.H. (2009). Experimental study of photocatalytic concrete products for air purification. *Building and Environment*, 44(12), 2463-2474. DOI: 10.1016/j.buildenv.2009.04.010.

[37] Jacoby, W.A., Blake, D.M., Noble, R.D., Koval, C.A. (1995). Kinetics of the oxidation of trichloroethylene in air via heterogeneous photocatalysis. *Journal of Catalysis*, 157(1), 87-96. DOI: 10.1006/jcat.1995.1270.

[38] Lim, T.H., Jeong, S.M., Kim, S.D., Gyenis, J. (2000). Photocatalytic decomposition of NO by TiO2 particles. *Journal of Photochemistry and Photobiology A: Chemistry*, 134(3), 209-217. DOI: 10.1016/S1010-6030(00)00265-3.

[39] Al-Jemeli, M., Mahmoud, M.A., Majdi, H.S., Abid, M.F., Abdullah, H.M., Abdul Razak, A.A. (2021). Degradation of Anti-Inflammatory Drugs in Synthetic Wastewater by Solar Photocatalysis. *Catalysts*, 11(11), 1330. DOI: 10.3390/catal11111330.

[40] Abid, M.F., Ebrahim, M., Nafi, O., Hussain, L., Maneual, N., Sameer, A. (2014). Designing and operating a pilot plant for purification of industrial wastewater from toxic organic compounds by utilizing solar energy. *Korean Journal of Chemical Engineering*, 31(7), 1194-1203. DOI: 10.1007/s11814-014-0052-0.

[41] Kim, I.K. (2014). Degradation of a Refractory Organic Contaminant by Photocatalytic Systems. *Journal of Power System Engineering*, 18(6), 133-139. DOI: 10.9726/kspse.2014.18.6.133.

[42] Kim, I.K., Huang, C.P., Chiu, P.C. (2001). Sonochemical decomposition of dibenzothiophene in aqueous solution. *Water Research*, 35(18), 4370-4378. DOI: 10.1016/S0043-1354(01)00176-2.